

Article

# Evaluation of CLDAS and GLDAS Datasets for Near-Surface Air Temperature over Major Land Areas of China

Shuai Han <sup>1,2,3,4</sup>, Buchun Liu <sup>1,2,3,\*</sup>, Chunxiang Shi <sup>4,\*</sup>, Yuan Liu <sup>1,2,3</sup>, Meijuan Qiu <sup>1,2,3</sup> and Shuai Sun <sup>4</sup>

<sup>1</sup> Institute of Environment and Sustainable Development in Agriculture, Chinese Academy of Agricultural Sciences, Beijing 100081, China; hans@cma.gov.cn (S.H.); liuyuan@caas.cn (Y.L.); qmjcams@163.com (M.Q.)

<sup>2</sup> National Engineering Laboratory of Efficient Crop Water Use and Disaster Reduction, Beijing 100081, China

<sup>3</sup> Key Laboratory of Agricultural Environment, Ministry of Agriculture, Beijing 100081, China

<sup>4</sup> National Meteorological Information Center, Beijing 100081, China; sunshuai@cma.gov.cn

\* Correspondence: liubuchun@caas.cn (B.L.); shicx@cma.gov.cn (C.S.)

Received: 25 April 2020; Accepted: 23 May 2020; Published: 25 May 2020



**Abstract:** As one of the most principal meteorological factors to affect global climate change and human sustainable development, temperature plays an important role in biogeochemical and hydrosphere cycle. To date, there are a wide range of temperature data sources and only a detailed understanding of the reliability of these datasets can help us carry out related research. In this study, the hourly and daily near-surface air temperature observations collected at national automatic weather stations (NAWS) in China were used to compare with the China Meteorological Administration (CMA) Land Data Assimilation System (CLDAS) and the Global Land Data Assimilation System (GLDAS), both of which were developed by using the advanced multi-source data fusion technology. Results are as follows. (1) The spatial and temporal variations of the near-surface air temperature agree well between CLDAS and GLDAS over major land of China, except that spatial details in high mountainous areas were not sufficiently displayed in GLDAS; (2) The near-surface air temperature of CLDAS were more significantly correlated with observations than that of GLDAS, but more caution is necessary when using the data in mountain areas as the accuracy of the datasets gradually decreases with increasing altitude; (3) CLDAS can better illustrate the distribution of areas of daily maximum above 35 °C and help to monitor high temperature weather. The main conclusion of this study is that CLDAS near-surface air temperature has a higher reliability in China, which is very important for the study of climate change and sustainable development in East Asia.

**Keywords:** near-surface air temperature; land data assimilation; CLDAS; GLDAS; evaluation

## 1. Introduction

Global warming and climate change are currently the world's most pressing issues [1], which is increasing the risk of extreme events, resulting in social and economic challenges [2]. The relationship between global climate change and human sustainable development, corporate social responsibility, corporate governance, business performance and the excellence model are closely. Big companies should take more social responsibilities, and policy-making should pay more attention to the long-term development of the company and humanity, which is more conducive to the common development of mankind [3]. Green and sustainable finance will enhance profit, productivity and performance and reduce financial fluctuation when being aware of the importance and the advantages brought by corporate social responsibility [4]. Meteorological datasets are the essential basis for climate

analysis and data application, particularly in agricultural, ecological, hydrological and environmental sciences [5]. Although the conventional station-based measurements can provide accurate values of the measured variables, these measurements can only present information on local scale [6,7]. They are unable to adequately depict spatial variations given the limited number and locations of stations [8]. Remote sensing data can achieve continuous orbit observation, but it is difficult to obtain high-resolution ground meteorological data in real time due to the restrictions of satellite orbit and detection band. Numerical model data can perform well in spatial-temporal simulation, but due to the influence of parameterization scheme, the simulation results often have certain uncertainty [9].

In the late 1980s, data assimilation and fusion techniques were proposed as a means of reconstructing historical meteorological data at high resolution [10,11]. Based on these techniques, different sources of meteorological data are fused to produce spatial-temporal, long-time series of gridded fusion datasets, which can make up for the shortcomings of different sources of data. These datasets provide the best estimate of meteorological elements at locations between observation stations, which is important for studies in regions where ground stations are lacking or sparse [12]. Ecological and hydrological models have high demand for gridded meteorological datasets that can be used as the model inputs to generate spatial distribution of the variable [13].

According to the differences of data assimilation and fusion techniques, the main gridded datasets include atmosphere assimilation datasets and land surface gridded fusion datasets. The atmosphere assimilation datasets elements contain air temperature, geopotential height, relative humidity, wind and other meteorological variables at different altitudes [10,11,14–16]. To date, the most widely used atmosphere assimilation datasets in the world include the National Centers for Environmental Prediction and the National Center for Atmospheric Research reanalysis data (NCEP/NCAR) [17], the European Center for Medium-Range Weather Forecasts (ECMWF) interim reanalysis data (ERA-Interim) [18], the Japanese 55-year reanalysis data (JRA-55) [19], and other datasets.

The land surface gridded fusion datasets including near-surface meteorological elements and soil variables have also developed rapidly, which have been widely used for agricultural drought monitoring, wild fire early warning and water resources management [20,21]. In early 2000s, NOAA first established the Global Land Data Assimilation System (GLDAS) [22]. After 2010, the China Meteorological Administration (CMA) Land Data Assimilation System (CLDAS) was completed covering East Asia areas [20,21,23,24]. Some of these elements have been evaluated, such as precipitation, and the results show that the CLDAS performs better than GLDAS [7]. Although the accuracy of near-surface air temperature of GLDAS and CLDAS have been assessed in limited areas [12], a comprehensive and detailed assessment over major land areas of China has not yet been carried out. The assessment of temperature datasets is an important part of climate change research, which provides valuable reference and practical significance for understanding regional temperature change and promoting sustainable development [25]. In this study, the accuracy and applicability of CLDAS and GLDAS near-surface air temperature datasets over major land areas of China are evaluated from different temporal and spatial perspectives by using ground automatic weather station observation data. According to the assessment conclusion, it will help researchers to select appropriate datasets for climate change research, agricultural and ecological simulation research, water and energy interaction research, environmental protection and sustainable development research. At the same time, it will also help to guide further innovations and improvements in these datasets.

## 2. Materials and Methods

### 2.1. GLDAS Near-Surface Air Temperature Data Product

GLDAS implements the land information system (LIS) [26], a land data assimilation system that consists of multiple land surface models, to integrate observation-based data and generate land surface state (e.g., soil moisture and surface temperature) and flux (e.g., evaporation and sensible heat flux) variables. Currently, the GLDAS runs four land surface models (LSMs): Mosaic, Noah, CLM and

VIC [27]. The temporal resolutions of the GLDAS products were 3-hourly and monthly (generated through averaging the 3-hour product). The spatial resolutions were  $1.0^\circ$  (from 1979 to present) using the four models and  $0.25^\circ$  (from 2000 to present) using the Noah model. GLDAS-2 was released recently, which uses the global meteorological forcing datasets from Princeton University to create more climatologically consistent datasets that cover an extended period from 1948 to 2010 [28]. In this study, the GLDAS version 1 datasets (Table 1) were used, which were downloaded from the NASA Goddard Earth Sciences Data and Information Services Center (GES DISC) (<https://ldas.gsfc.nasa.gov/data>). The datasets were in the gridded binary (GRIB) format, containing 22 physical variables at 3-hour intervals with the horizontal resolution of  $0.25^\circ$ . The spatial extension of the datasets ranges from  $60^\circ\text{S}$  to  $90^\circ\text{N}$  (latitude) and from  $180^\circ\text{W}$  to  $180^\circ\text{E}$  (longitude) in the geographic coordinate system. Three-hour near-surface air temperatures (kelvins) were extracted from GLDAS datasets.

### 2.2. CLDAS Near-Surface Air Temperature Data Product

CLDAS datasets mainly include forcing datasets and land surface datasets. The forcing datasets were developed by using multi-grid variational analysis technique [10], terrain correction algorithm [24] and discrete ordinates radiative transfer (DISORT) model [29] to blend station observations, numerical forecast data and satellite data. The land surface datasets were developed by running the community land model version 3.5 (CLM3.5) [30], the common land model (CoLM) [31] and Noah LSM with four physics options (Noah MP) [32] to produce various soil variables like soil temperature, soil moisture, evapotranspiration, surface heat flux, etc. The temporal resolutions of the CLDAS datasets were hourly and daily (generated through averaging the hourly product). The spatial resolution was  $0.0625^\circ$  (from 2008 to present). In this study, the CLDAS version 2 datasets (Table 1) released at 2016 in  $0.0625^\circ \times 0.0625^\circ$  grids and at hourly intervals were used, which were downloaded from the China Meteorological Data Service Center (CMDSC) (<http://data.cma.cn>) [9,20,23,24,33,34]. The datasets were in the NETCDF (NC) format. The spatial extension of the datasets ranges from  $0^\circ$  to  $65^\circ\text{N}$  (latitude) and from  $60^\circ\text{E}$  to  $160^\circ\text{E}$  (longitude) in the geographic coordinate system. Hourly near-surface air temperatures (kelvins) were extracted from CLDAS datasets.

### 2.3. National and Regional Automatic Weather Station Observations

National automatic weather station (NAWS) observations were provided by the National Meteorological Information Center (NMIC), CMA, including observations collected from more than 2380 stations in China (Figure 1a). These automatic weather stations maintained by the China Meteorological Administration were regularly calibrated and the observations were regarded as reliable [35]. In this study, hourly near-surface air temperature observations from 2010 to 2015 were used to verify the gridded CLDAS and GLDAS datasets. Meanwhile, the observations of the regional automatic weather station (RAWS) in Sichuan Province were also used for the assessment of daily maximum and minimum temperature (Figure 1b).

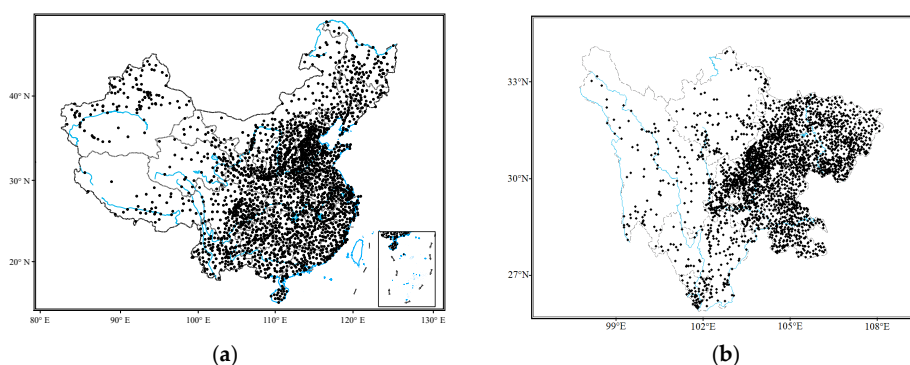


**Figure 1.** (a) Distribution of national automatic weather stations (NAWS) in China; (b) distribution of NAWS and regional automatic weather station (RAWS) in Sichuan Province.

Detailed properties of various data used in this study and their spatial-temporal resolutions as well as the period of coverage are listed in Table 1.

**Table 1.** Datasets information of NAWS, RAWS, China Meteorological Administration (CMA) Land Data Assimilation System (CLDAS), and Global Land Data Assimilation System (GLDAS)

Datasets	NAWS Observations	RAWS Observations	CLDAS	GLDAS
Data type	Point	Point	Grid	Grid
Spatial coverage	over major land areas of China	Sichuan Province	60°E–160°E 0°–65°N	180°W–180°E 60°S–90°N
Spatial resolution	more than 2400 ground stations	more than 770 ground stations	0.0625°	0.25°
Temporal coverage	From 2008 to present	From 2008 to present	From 2008 to present	From 1979 to present
Temporal resolution	hourly	hourly	hourly	3-hourly
Unit	°C	°C	K	K

#### 2.4. Methodology

To evaluate the CLDAS and GLDAS near-surface air temperature, all the available air temperature data from NAWS recorded from 2010 to 2015 and data from RAWS recorded in July of 2018 were obtained. Near-surface air temperature were extracted from the gridded CLDAS and GLDAS datasets for all the NAWS and RAWS locations based on the latitude and longitude information of these stations and compared with observations using the agreement indices given below.

The following agreement indices, i.e., bias, root-mean-square error (RMSE), correlation coefficient (COR), mean absolute error (MAE), temperature accuracy (TA), were implemented to compare NAWS observations with the CLDAS and GLDAS near-surface air temperature data. These five indices were defined as:

$$\text{Bias} = \frac{1}{N} \sum_{i=1}^N (G_i - O_i) \quad (1)$$

$$\text{RMSE} = \sqrt{\frac{1}{N} \sum_{i=1}^N (G_i - O_i)^2} \quad (2)$$

$$\text{COR} = \frac{\sum_{i=1}^N (G_i - \bar{G}_i)(O_i - \bar{O}_i)}{\sqrt{\sum_{i=1}^N (G_i - \bar{G}_i)^2} \sqrt{\sum_{i=1}^N (O_i - \bar{O}_i)^2}} \quad (3)$$

$$\text{MAE} = \frac{1}{N} \sum_{i=1}^N |(G_i - O_i)| \quad (4)$$

$$\text{TA}_j = \frac{N_{ri}}{N_{fi}} \quad (5)$$

where  $O_i$  indicates observations at weather station  $i$  (true values),  $G_i$  denotes the GLDAS or CLDAS data interpolated to a given station  $i$ ,  $N$  was the total number of stations used for verification.  $N_{ri}$  was the number of stations with correct near-surface air temperature,  $N_{fi}$  was the total number of stations,  $j = 1.5$  and  $\text{TA}_{1.5}$  indicates the accuracy rate of temperature, i.e., the percentage of samples with absolute error  $\leq 1.5$  °C.

Bi-linear interpolation method was implemented in the present study. The algorithm is written as:

$$Z(I_1, J) = \frac{J - J_2}{J_1 - J_2} Z(I_1, J_1) + \frac{J - J_1}{J_2 - J_1} Z(I_1, J_2) \quad (6)$$

$$Z(I_2, J) = \frac{J - J_2}{J_1 - J_2} Z(I_2, J_1) + \frac{J - J_1}{J_2 - J_1} Z(I_2, J_2) \quad (7)$$

A linear interpolation was further conducted along the J-direction:

$$Z(I, J) = \frac{I - I_2}{I_1 - I_2} Z(I_1, J) + \frac{I - I_1}{I_2 - I_1} Z(I_2, J) \quad (8)$$

where  $Z(I_1, J_1)$ ,  $Z(I_1, J_2)$ ,  $Z(I_2, J_1)$  and  $Z(I_2, J_2)$  were values of the variable on the corresponding grids;  $Z(I_1, J)$  and  $Z(I_2, J)$  were results at  $I_1$  latitude and  $I_2$  latitude after the linear interpolation;  $Z(I, J)$  was the value at a specific station after the interpolation.

### 3. Results

#### 3.1. Comparative Analysis of Spatial-Temporal Distribution Characteristics

The daily mean near-surface air temperature from CLDAS and GLDAS on four dates, 15 January, 15 April, 15 July and 15 October in 2010 are shown in Figure 2. The four dates represent winter, spring, summer and autumn, respectively. Seasonal variation analysis reveals that the near-surface air temperature was obviously lower in winter with the temperature in the Tibetan Plateau and northeast China generally below minus 10 °C, and was higher in summer over entire China with the value above 30 °C in Xinjiang and southeast China. The near-surface air temperature of CLDAS and GLDAS has the same seasonal variation trend.

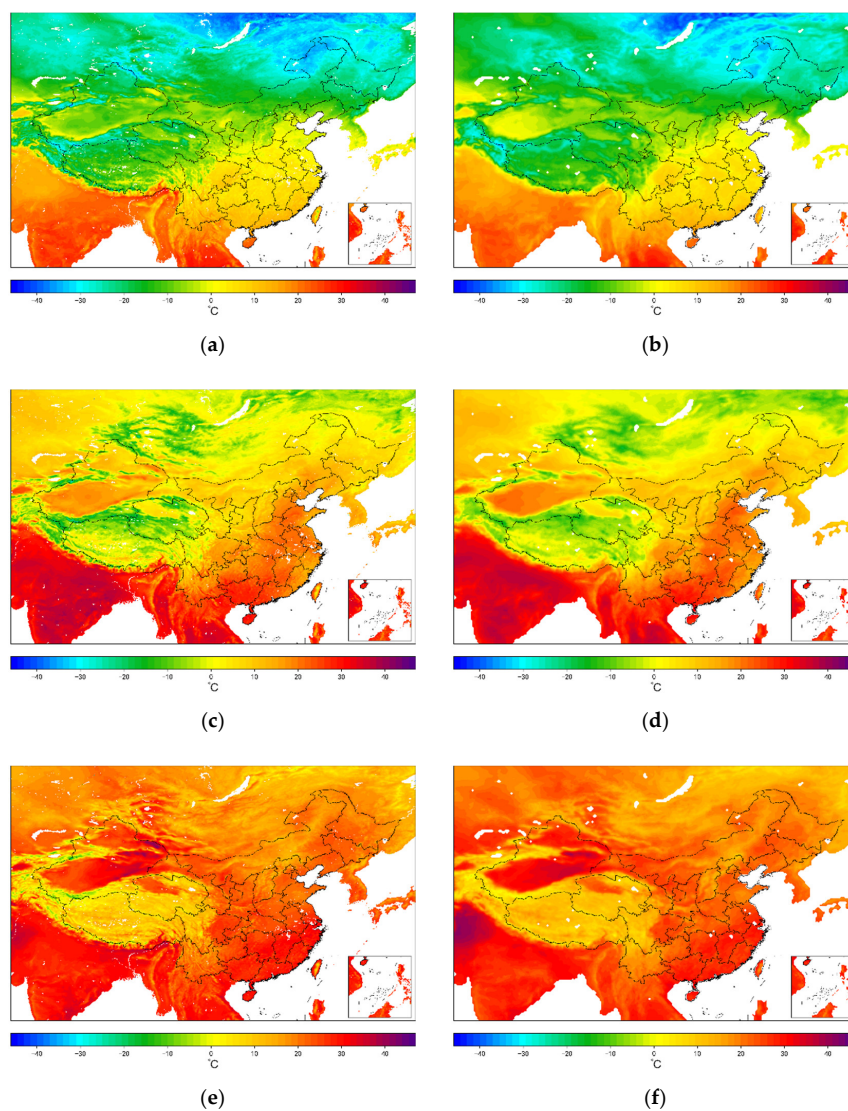
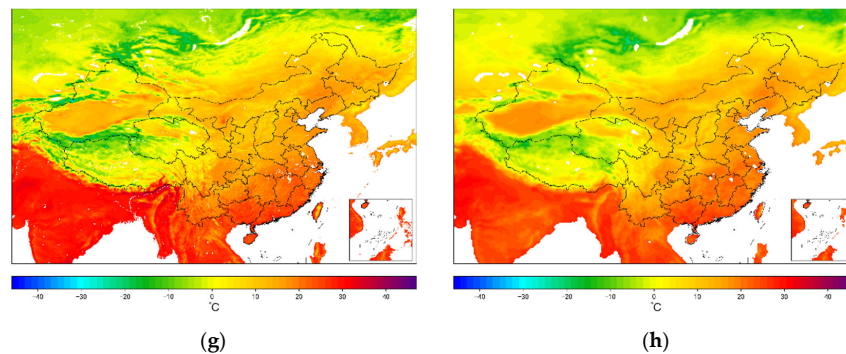


Figure 2. Cont.



**Figure 2.** Spatial distributions of near-surface air temperature. (a), (c), (e) and (g) represent the near-surface air temperature of CLDAS on January 15, April 15, July 15 and October 15, respectively; (b), (d), (f) and (h) represent the near-surface air temperature of the Global Land Data Assimilation System (GLDAS) on January 15, April 15, July 15 and October 15, respectively.

In the same season, the near-surface air temperature of both CLDAS and GLDAS is cold in northeastern and northwestern China and warm in southeastern China as expected. The near-surface air temperature is colder in the Tibetan region than in other regions year-round due to the high elevation of the Tibetan Plateau. Overall, the observed spatial patterns were well captured by both CLDAS and GLDAS. The spatial variability of the near-surface air temperature of CLDAS and GLDAS has a high consistency and the same order of magnitude. However, slight differences can be found at either local or regional scale. In southwest China, especially in high altitude areas such as Tibetan Plateau, Guizhou, Yunnan and Sichuan, the CLDAS data show more detailed local variations, while the GLDAS data present more spatially smoothed features, which was attributed to the large changes in topography and differences in spatial resolution.

### 3.2. Comparative Analysis of Daily Time Series

Time series of daily mean near-surface air temperature of observations, CLDAS and GLDAS during the year (1–365 Julian days) averaged over major land of China from 2010 to 2015 are displayed in Figure 3a, which shows that, the trend of both CLDAS and GLDAS over time in the year was basically consistent with the observations. However, CLDAS was generally closer to observations, while GLDAS underestimate for most of the year, especially in summer.

Time series of daily COR are displayed in Figure 3b. The COR of CLDAS were higher than that of GLDAS throughout the year. The COR between CLDAS and observations was largely within the range from 0.98 to 1 without distinct variability. In contrast, the COR between GLDAS and observations varied between 0.84 and 0.96 with fluctuations during the year, which reached a minimum in summer, demonstrating a distinct seasonal variation.

Time series of daily RMSE are displayed in Figure 3c. The RMSE of CLDAS was lower than that of GLDAS over the year. For CLDAS, the RMSE was largely distributed between 1–1.2 °C. For GLDAS, however, the RMSE was mainly concentrated between 3–3.5 °C.

Time series of daily bias are displayed in Figure 3d. It shows negative bias for both CLDAS and GLDAS, meanwhile, the bias of CLDAS was smaller than that of GLDAS all over the year. The bias between CLDAS and observations was about minus 0.1 °C, whereas the bias between GLDAS and observations varied between minus 0.6 °C–1.2 °C. The bias of CLDAS was more stable, while that of GLDAS was more fluctuant during the year.

In general, for the daily mean near-surface air temperature, CLDAS was closer to observations than GLDAS, with higher COR, lower RMSE and smaller bias.

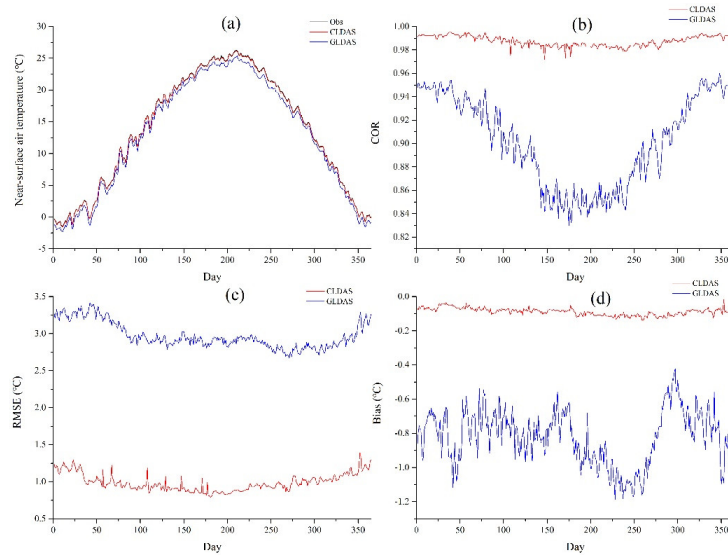


**Figure 3.** (a) Time series of daily mean near-surface air temperature; (b) time series of correlation coefficient (COR); (c) time series of RMSE; (d) bias time series. Daily average near-surface air temperature was averaged from 2010 to 2015.

### 3.3. Comparative Analysis of Daily Mean Diurnal Cycle

The daily mean (from 2010 to 2015) diurnal cycle of near-surface air temperature averaged over all NAWS observations, CLDAS and GLDAS are shown in Figure 4. The near-surface air temperature of observations, CLDAS and GLDAS all demonstrate distinct diurnal and seasonal variations.

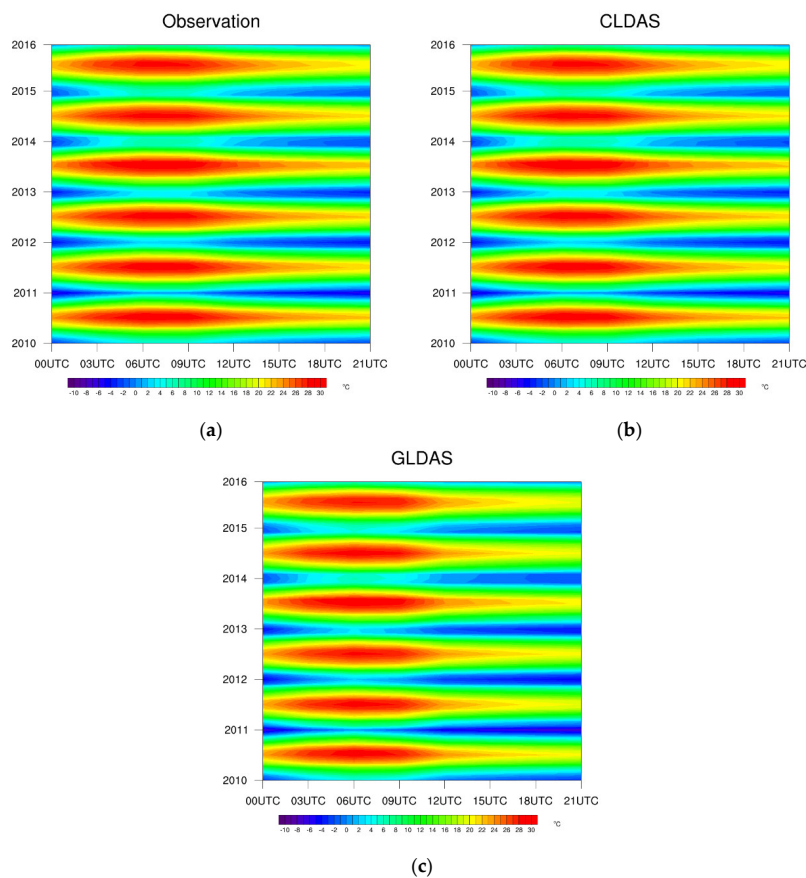


**Figure 4.** Hourly variations of near-surface air temperature in the period of 2010–2015. (a) Observations; (b) China Meteorological Administration (CMA) Land Data Assimilation System (CLDAS); (c) GLDAS.

Diurnal variations of COR for CLDAS and GLDAS are displayed in Figure 5. In general, the COR of CLDAS was higher than that of GLDAS. As shown in Figure 5a, the COR between CLDAS and observations was basically larger than 0.98 on daily scale, except the COR was slightly lower during 06–15 UTC in summer, when the value was between 0.96–0.98. As shown in Figure 5b, the COR between GLDAS and observations was also lower in summer than in other seasons. In summer, the COR decreases first from 00 UTC, reaches its lowest value of around 0.8 at 12 UTC and then increases, demonstrating a periodic change. The main possible reason for the low COR in summer may be that more high temperature days occur in summer, while the gridded datasets cannot accurately describe the maximum temperature.

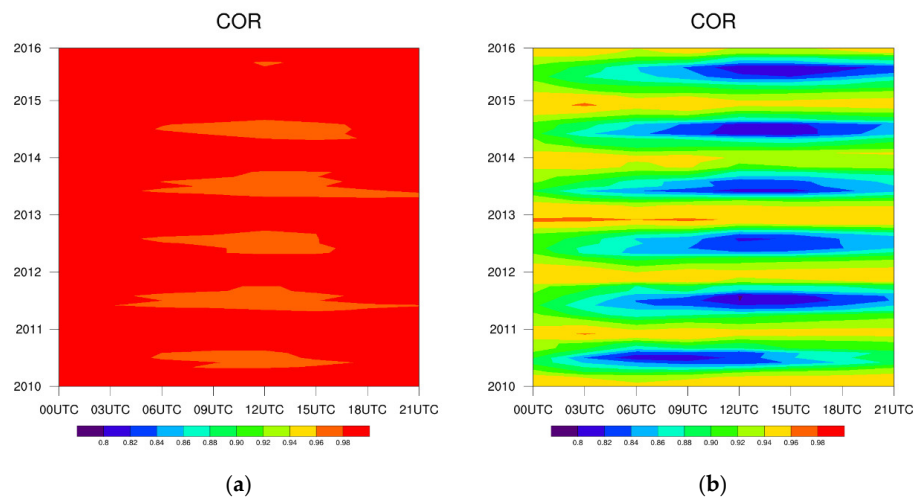


**Figure 5.** Diurnal variations of near-surface air temperature COR during 2010–2015. (a) CLDAS; (b) GLDAS.

Diurnal variations of RMSE for CLDAS and GLDAS are displayed in Figure 6. In general, the RMSE of CLDAS was lower than that of GLDAS. As shown in Figure 6a, the RMSE of CLDAS on daily scale was largely distributed between 0.6–1.2 °C and generally small in summer during 00–03UTC and 18–21 UTC, except that it was larger than 1.2 °C during 00–03UTC and 18–21 UTC only in several specific winters. As shown in Figure 6b, the RMSE of GLDAS on daily scale was largely distributed higher than 2.7 °C, except that it was small in summer with the value of 2.4–2.7 °C during 00–09 UTC.

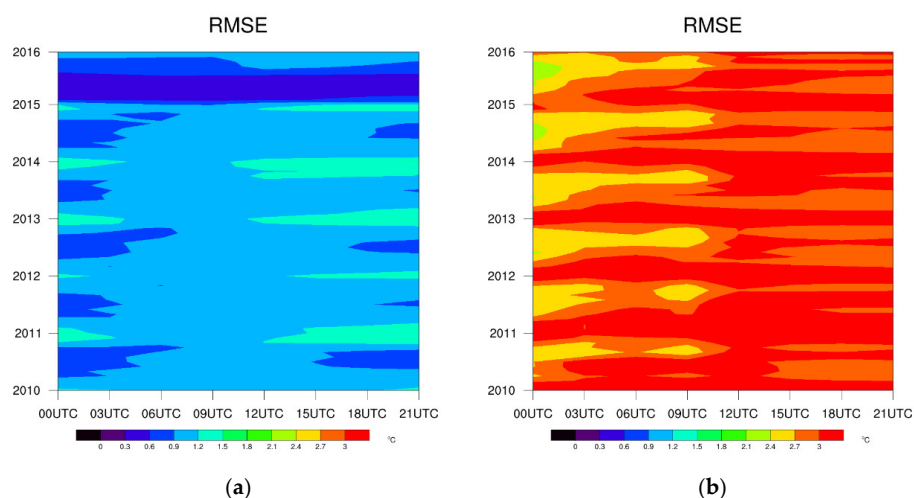


**Figure 6.** Diurnal variations of near-surface air temperature root-mean-square error (RMSE) during 2010–2015. (a) CLDAS; (b) GLDAS.

Diurnal variations of bias for CLDAS and GLDAS are displayed in Figure 7. In general, the bias of CLDAS was lower than that of GLDAS. As shown in Figure 7a, the bias of CLDAS was small with the value ranging between minus 0.4 °C–0.8 °C. In all the seasons, the bias was almost always positive with the value varying between 0 °C–0.8 °C during 00:00–08:00 UTC, and it was negative in other time of the day. As shown in Figure 7b, the positive bias of GLDAS was around 0 °C–0.4 °C during 06:00–09:00 UTC and the positive bias was more distinct in summer. In other time of the day, the bias was negative with the value basically smaller than minus 1 °C.

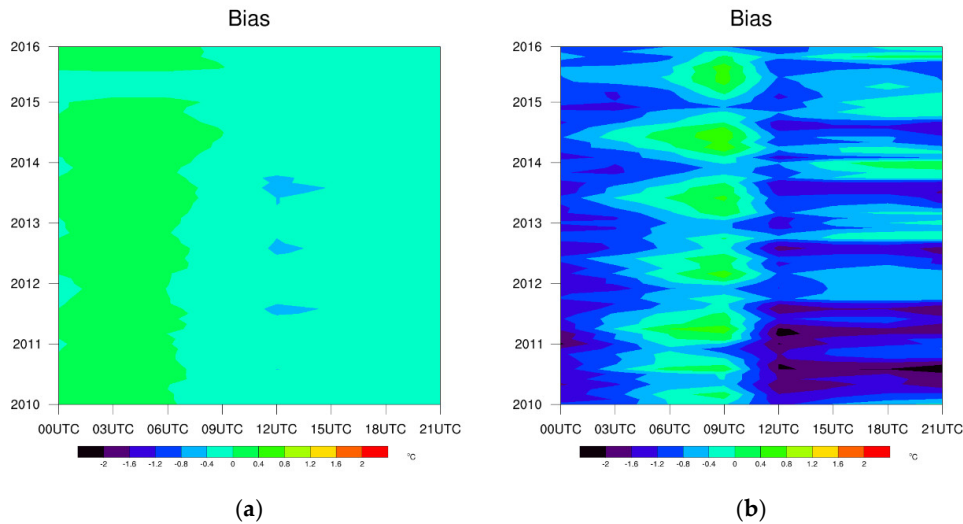


Figure 7. Diurnal variations of near-surface air temperature bias during 2010–2015. (a) CLDAS; (b) GLDAS.

3.4. Comparative Analysis on Each Station

The COR for CLDAS and GLDAS at local stations of China are displayed in Figure 8. On most stations, the COR of CLDAS was higher than that of GLDAS. The COR of both CLDAS and GLDAS decreased from east to west. As shown in Figure 8a, for CLDAS, the COR of most stations were above 0.99, except for Yunnan, the Western Hengduan and the Tibetan Plateau. As shown in Figure 8b, for GLDAS, the highest COR larger than 0.98 occurs in Shandong and its adjacent provinces. The value decreases to 0.97–0.98 in central China and was lower than 0.97 in most stations of central-western China.

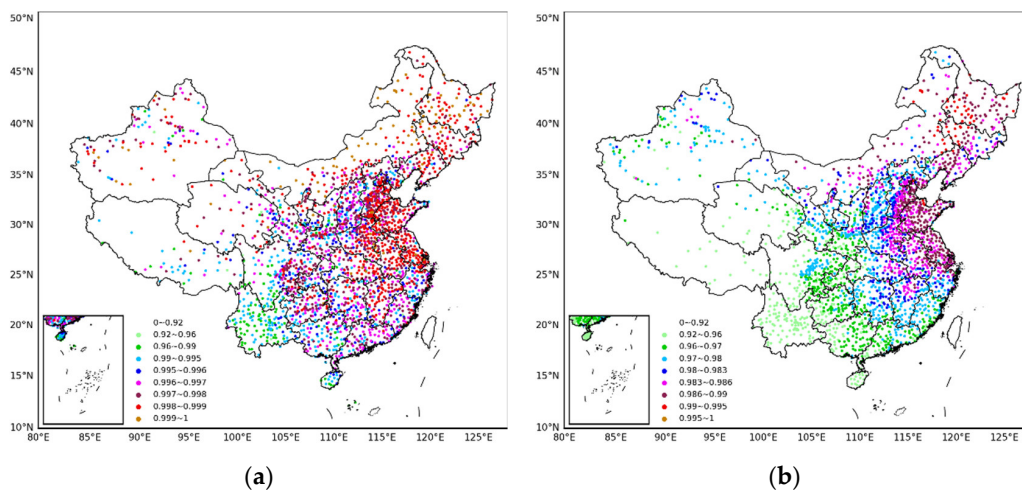


Figure 8. Spatial distribution of COR. (a) CLDAS; (b) GLDAS.

The RMSE for CLDAS and GLDAS at local stations of China are displayed in Figure 9. On most stations, the RMSE of CLDAS was lower than that of GLDAS. The results for the CLDAS are presented

in Figure 9a, which shows that the RMSE at most stations was smaller than 1 °C. In Xinjiang, Yunnan, the Tibetan Plateau and western Sichuan, the RMSE varies between 1 °C–1.4 °C. Meanwhile, the RMSE can be greater than 3 °C at sporadic stations, where measurement failure may possibly be the reason. The results for GLDAS are displayed in Figure 9b, which shows that the RMSE gradually increases from southeast to northwest over major land of China. Specifically, the RMSE was smaller than 2 °C in central and eastern China and the value can be lower than 1.5 °C at some stations, but the RMSE was higher than 3 °C in the western region.

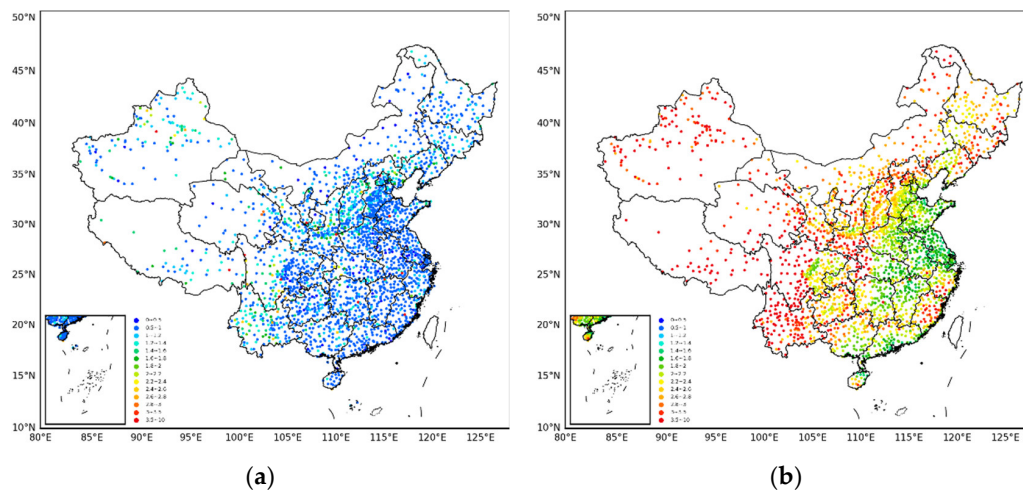


Figure 9. Spatial distribution of RMSE. (a) CLDAS; (b) GLDAS.

The bias for CLDAS and GLDAS at local stations of China are displayed in Figure 10. On the whole, the bias of CLDAS was smaller than that of GLDAS, especially in southwest China, such as Tibetan Plateau, Yunnan and Sichuan and southeast China, such as Fujian and Zhejiang. As shown in Figure 10a, the bias of CLDAS was within minus 0.5 °C–0.5 °C at most stations and there was no significant difference among provinces. As shown in Figure 10b, the biases of GLDAS in southern Hebei, Henan, Hubei, Hunan and western Shandong were smaller than that in other provinces and large biases were concentrated along areas surrounding Sichuan Basin and over the Tibetan Plateau. The GLDAS was generally reliable over plains of China, but it has large negative bias in complex terrain area (such as Sichuan and Chongqing) and high-elevation area (Tibetan Plateau).

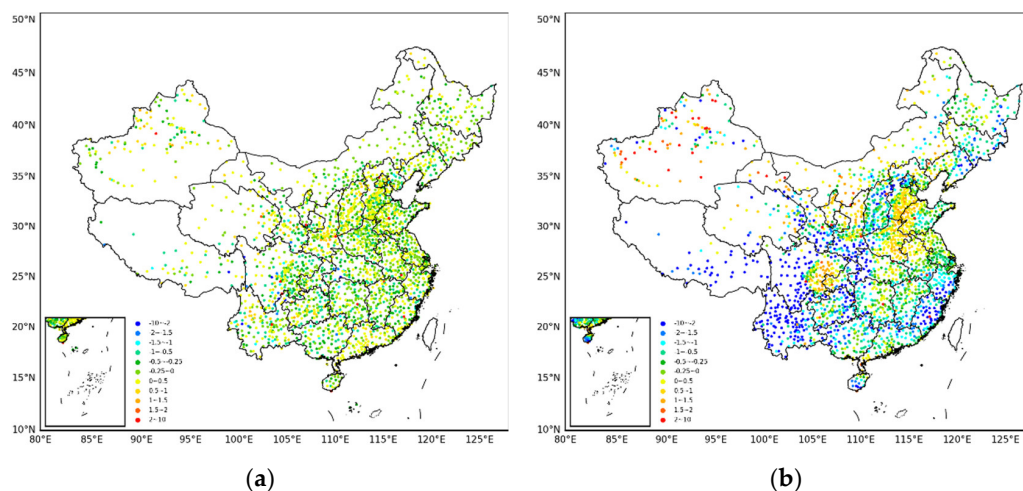
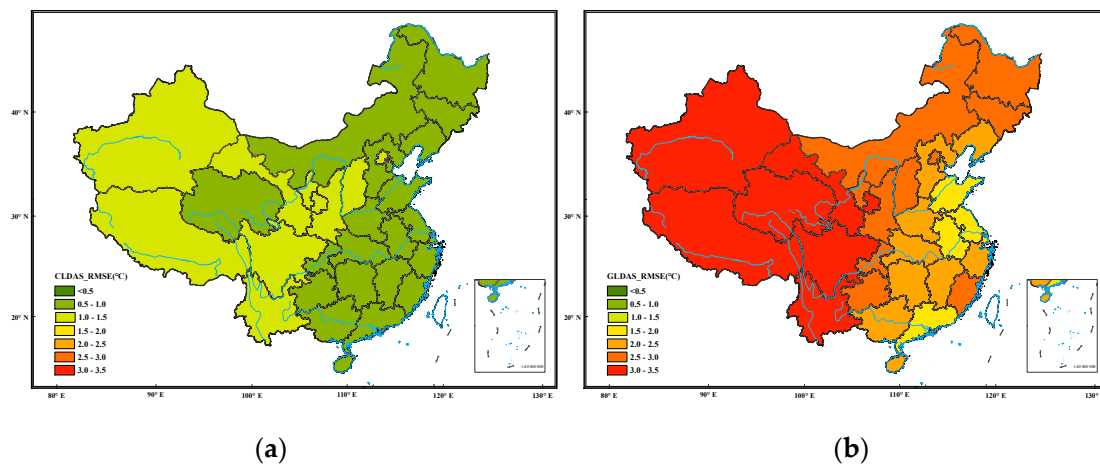


Figure 10. Spatial distribution of bias. (a) CLDAS; (b) GLDAS.

### 3.5. Comparative Analysis for Each Province

Province is the administrative unit of China and its division is mostly based on the geographical and climatic attributes. Therefore, it was necessary to carry out the assessment from the perspective of provinces. All the national automatic weather stations in China were grouped based on their province attributes and the samples of each province were used for statistical analysis. bias, RMSE and COR of CLDAS and GLDAS with observations were calculated for each province. Spatial distribution of RMSE for individual provinces of China is presented in Figure 11. For both CLDAS (Figure 11a) and GLDAS (Figure 11b), the data quality was better in eastern China than in western China. The RMSE of CLDAS was smaller than that of GLDAS in the same province.

The evaluation results of CLDAS and GLDAS in each province are listed in Table 2. The COR of CLDAS was above 0.99 at most provinces, while the COR of GLDAS was above 0.95 at all provinces except Yunnan and the Tibetan Plateau. The RMSE of CLDAS was smaller than 1 °C in more than two-thirds of the provinces, while the RMSE of GLDAS was smaller than 2.5 °C in more than half of the provinces. The absolute value of bias of CLDAS was within 0.3 °C, while the absolute values of bias of GLDAS was mostly within 1 °C. Evaluation results indicate that CLDAS was closer to the observations than GLDAS in all provinces.



**Figure 11.** Spatial distribution of RMSE in individual provinces of China. (a) CLDAS; (b) GLDAS.

### 3.6. Comparative Analysis at Different Altitude

In order to investigate the relationship between the evaluation results and altitude, the near-surface air temperature of different altitude were evaluated. Since the highest altitude of the stations participating the evaluation was 4800 m and few stations were located above 2000 m, the altitude was divided into three levels, i.e., below 1000 m, 1000 m to 2000 m and above 2000 m, for evaluation in this study. There were 1782 stations located below 1000 m, 423 stations located between 1000 m to 2000 m and 165 stations located above 2000 m. As shown in Figure 12, with the increase of altitude and the decrease of the number of stations participating in the evaluation, the accuracy of CLDAS and GLDAS gradually decreases and the evaluation indices become worse. However, CLDAS performs better than GLDAS at all altitudes.

As shown in Figure 12a, for stations below 1000 m, the COR was 0.999 for CLDAS and 0.977 for GLDAS. For stations between 1000 m and 2000 m, the COR was 0.995 for CLDAS and 0.964 for GLDAS. For stations above 2000 m, the COR was 0.992 for CLDAS and 0.939 for GLDAS. With the increase of altitude, the COR of CLDAS and GLDAS both decrease, but GLDAS decreases more significantly than CLDAS. Overall, the COR of CLDAS was greater than that of GLDAS at all altitudes.

**Table 2.** The evaluation results of CLDAS and GLDAS in each province.

Province/Index	CLDAS			GLDAS		
	COR	RMSE (°C)	Bias (°C)	COR	RMSE (°C)	Bias (°C)
Beijing	0.99	1.12	0.11	0.98	2.72	-1.11
Tianjin	0.99	0.86	-0.08	0.99	2.01	-0.46
Hebei	0.99	0.93	-0.06	0.98	2.33	0.10
Shanxi	0.99	1.06	0.06	0.98	2.6	-0.87
Inner Mongolia	0.99	0.83	-0.08	0.99	2.79	-0.01
Liaoning	0.99	0.96	-0.11	0.99	2.46	-0.52
Jilin	0.99	0.94	-0.08	0.99	2.77	-0.96
Heilongjiang	0.99	0.94	-0.06	0.99	2.70	-0.56
Shanghai	0.99	0.60	-0.17	0.99	1.70	-0.59
Jiangsu	0.99	0.64	-0.11	0.99	1.69	-0.22
Zhejiang	0.99	0.81	-0.14	0.98	2.26	-1.23
Anhui	0.99	0.75	-0.06	0.98	1.92	-0.14
Fujian	0.99	0.79	-0.07	0.97	2.64	-1.59
Jiangxi	0.99	0.76	-0.22	0.98	2.06	-0.63
Shandong	0.99	0.84	-0.06	0.99	1.98	-0.02
Henan	0.99	0.81	-0.17	0.98	2.13	0.17
Hubei	0.99	0.79	-0.23	0.98	2.34	-0.92
Hunan	0.99	0.86	-0.17	0.97	2.23	-0.56
Guangdong	0.99	0.68	0.15	0.96	2.00	-0.59
Guangxi	0.99	0.86	-0.28	0.96	2.44	-1.06
Hainan	0.99	0.80	-0.03	0.95	2.09	-0.94
Chongqing	0.99	0.87	-0.28	0.96	2.78	-0.83
Sichuan	0.99	1.04	-0.23	0.95	3.93	-2.03
Guizhou	0.99	0.81	-0.12	0.96	2.63	-1.11
Yunnan	0.98	1.17	-0.12	0.93	4.05	-2.99
Xizang	0.99	1.19	-0.27	0.92	6.04	-4.66
Shaanxi	0.99	1.03	0.09	0.97	2.91	-0.66
Gansu	0.99	1.07	-0.06	0.97	3.09	-0.91
Qinghai	0.99	0.96	0.1	0.95	3.72	-1.21
Ningxia	0.99	1.09	0.08	0.98	2.71	0.47
Xinjiang	0.99	1.22	0.10	0.97	3.71	0.21
China	0.99	0.91	-0.08	0.97	2.69	-0.85

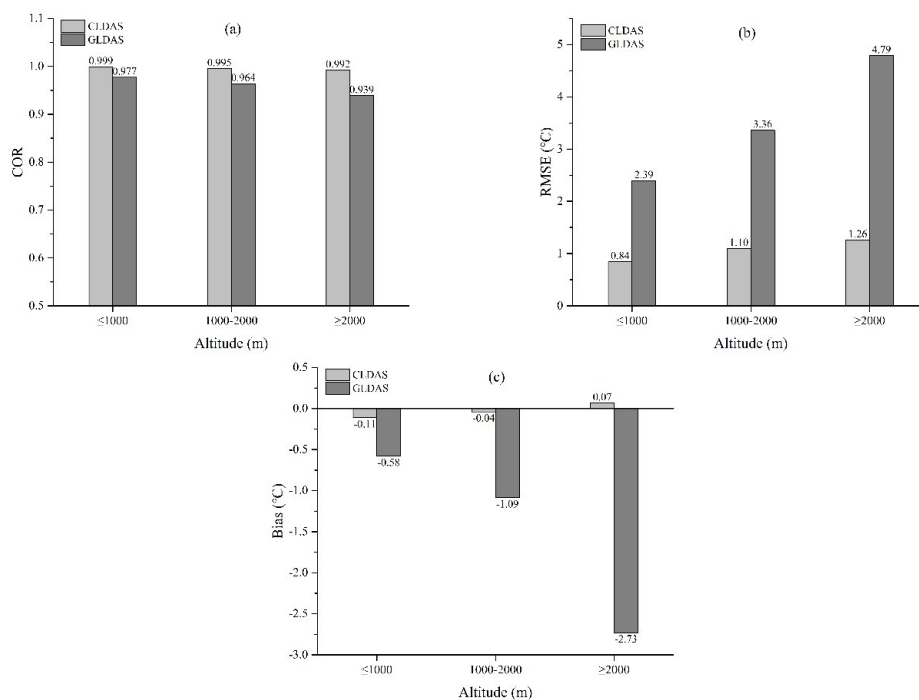


**Figure 12.** The (a) COR; (b) RMSE; and (c) bias of CLDAS and GLDAS at different altitudes.

As shown in Figure 12b, for stations below 1000 m, the RMSE was 0.84 °C for CLDAS and 2.39 °C for GLDAS. For stations between 1000 m and 2000 m, the RMSE was 1.1 °C for CLDAS and 3.36 °C for GLDAS. For stations above 2000 m, the RMSE was 1.26 °C for CLDAS and 4.79 °C for GLDAS. With the increase of altitude, the RMSE of CLDAS and GLDAS both increase, but GLDAS increases more significantly than CLDAS. Overall, the RMSE of CLDAS was smaller than that of GLDAS at all altitudes.

As shown in Figure 12c, for stations below 1000 m, the bias was minus 0.11 °C for CLDAS and minus 0.58 °C for GLDAS. For stations between 1000 m and 2000 m, the bias was minus 0.04 °C for CLDAS and minus 1.09 °C for GLDAS. For stations above 2000 m, the bias was 0.07 °C for CLDAS and minus 2.73 °C for GLDAS. With the increase of altitude, the bias of GLDAS increases obviously, while that of CLDAS was stable. The bias of CLDAS was smaller than that of GLDAS at all altitudes.

### 3.7. Evaluation of Daily Maximum and Minimum Temperature

Under the background of climate change, extreme weather and climate events occur frequently, which have a serious impact on the sustainable development of society. The applicability evaluation of the datasets in extreme high temperature has important reference value for other scholars to use the datasets to carry out disaster risk assessment and prevention, economic and social sustainable development and other related research. In 2018, China experienced a continuous high temperature process. In July, temperatures in most areas of China was higher than that during the same period of normal years and broke the local historical records at many places. In order to further evaluate whether the continuous high temperature can be represented in gridded products, the data from July 1 to July 31 in 2018 were analyzed.

The maximum and minimum temperature used in the study were defined as the daily highest and lowest near-surface air temperature during 20–20 BJT in gridded datasets and observations.

The results of maximum temperature of CLDAS and GLDAS are shown in Figure 13a,c, respectively. The COR was 0.96 for CLDAS and 0.84 for GLDAS. The bias was minus 0.71 °C for CLDAS and minus 3.39 °C for GLDAS. The MAE was 1.10 °C for CLDAS and 3.81 °C for GLDAS. The RMSE was 1.49 °C for CLDAS and 3.52 °C for GLDAS. In terms of accuracy, there were 78% of the samples have the bias within 1.5 °C for CLDAS, while only 26% of the samples had a bias within 1.5 °C for GLDAS. The results of minimum temperature of CLDAS and GLDAS are shown in Figure 13b,d, respectively. The COR was 0.98 for CLDAS and 0.91 for GLDAS. The bias was 0.10 °C for CLDAS and minus 2.65 °C for GLDAS. The MAE was 0.66 °C for CLDAS and 2.99 °C for GLDAS. The RMSE was 1.01 °C for CLDAS and 2.82 °C for GLDAS. In terms of accuracy, 91% of the samples showed a bias within 1.5 °C for CLDAS, while only 40% of the samples showed a bias within 1.5 °C for GLDAS. This showed that CLDAS was closer to observations in both maximum and minimum temperature than GLDAS and the accuracy of CLDAS was higher than that of GLDAS. The accuracy of both CLDAS and GLDAS in minimum temperature was higher than that in maximum temperature.

The numbers of high temperature stations were also compared between the gridded datasets and observations. It was found that the number of stations with maximum temperature in the range of 35 °C–38 °C for CLDAS was basically the same as that for observations (Figure 14a), while the number of stations for GLDAS was less than observations, which suggests that CLDAS was well indicative of high temperature ranging from 35 °C to 38 °C. However, the number of stations with maximum temperature ranging from 38 °C to 40 °C (Figure 14b) and above 40 °C (Figure 14c) for CLDAS and GLDAS were both smaller than that for observations. The highest daily maximum temperature of all stations in this region was selected to evaluate the quality of CLDAS and GLDAS in extreme high temperature. As shown in Figure 14d, the observed highest daily maximum temperature in the whole study region was above 40 °C in most time of July and can reach up to 50 °C occasionally. Comparison of highest daily maximum temperature suggests that both CLDAS and GLDAS was lower than observations, and CLDAS was closer to observations than GLDAS.

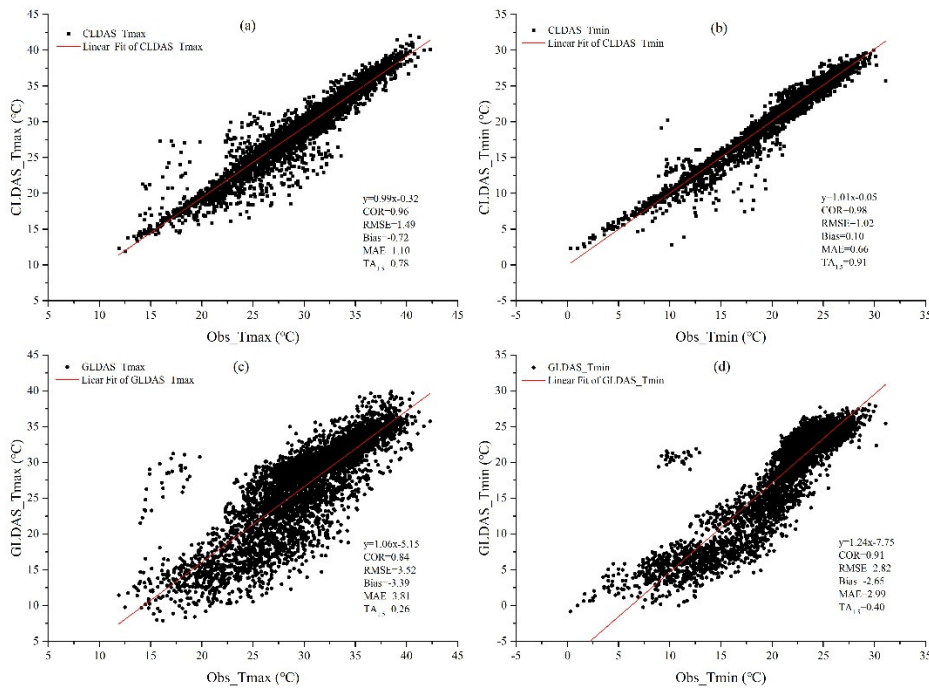


**Figure 13.** Scatter plots of daily maximum and minimum near-surface air temperature for CLDAS and GLDAS. (a) Daily maximum near-surface air temperature for CLDAS; (b) daily minimum near-surface air temperature for CLDAS; (c) daily maximum near-surface air temperature for CLDAS; (d) daily minimum near-surface air temperature for CLDAS.

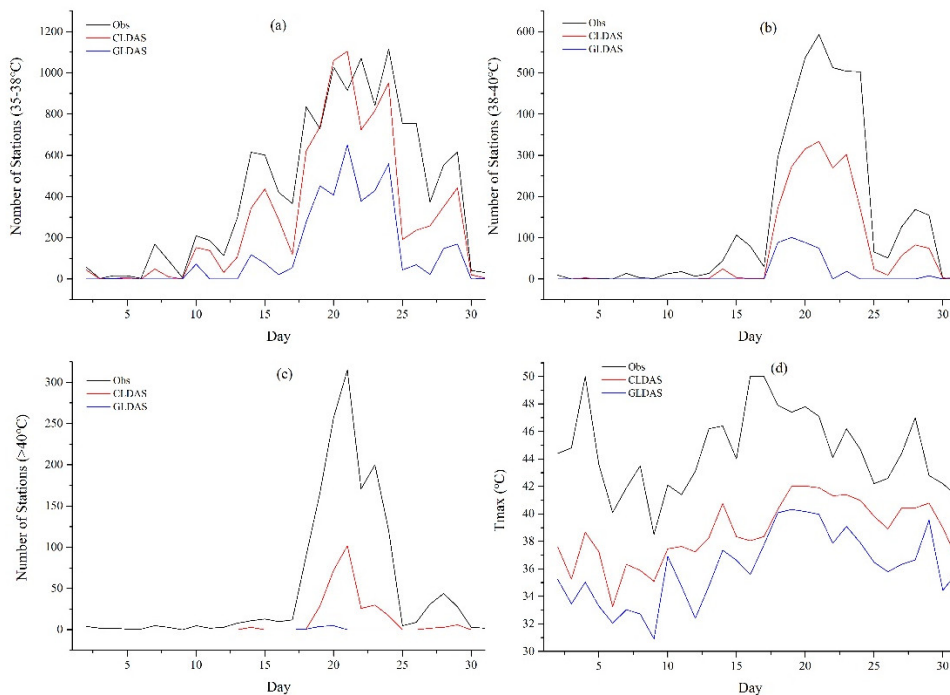


**Figure 14.** (a) Daily variations of number of high-temperature (35 °C–38 °C) stations in July 2018 for observations, CLDAS and GLDAS; (b) daily variations of number of high-temperature (38 °C–40 °C) stations in July 2018 for observations, CLDAS and GLDAS; (c) daily variations of number of high-temperature (above 40 °C) stations in July 2018 for observations, CLDAS and GLDAS; (d) highest daily maximum temperature in July 2018 for observations, CLDAS and GLDAS.

The number of high temperature stations reached the peak on 20 July in 2018. The geographic distributions of daily maximum temperature stations on this day is shown in Figure 15. The daily maximum temperature distribution of observations is shown in Figure 15a, which indicates that the maximum temperature in most east areas of the Hengduan Mountain was above 35 °C and can reach up to 38 °C and even exceeded 40 °C in some places. The daily maximum temperature distribution of CLDAS shown in Figure 15b was generally consistent with that of observations, except the area with high temperature higher than 38 °C of CLDAS was smaller than that of observations. In general, CLDAS can well illustrate the high temperature distribution and was able to monitor the high temperature weather. The daily maximum temperature distribution of GLDAS is shown in Figure 15c, which cannot realistically represent changes in high temperature areas. Further improvements are needed for GLDAS data before it can be applied for extreme high temperature study.

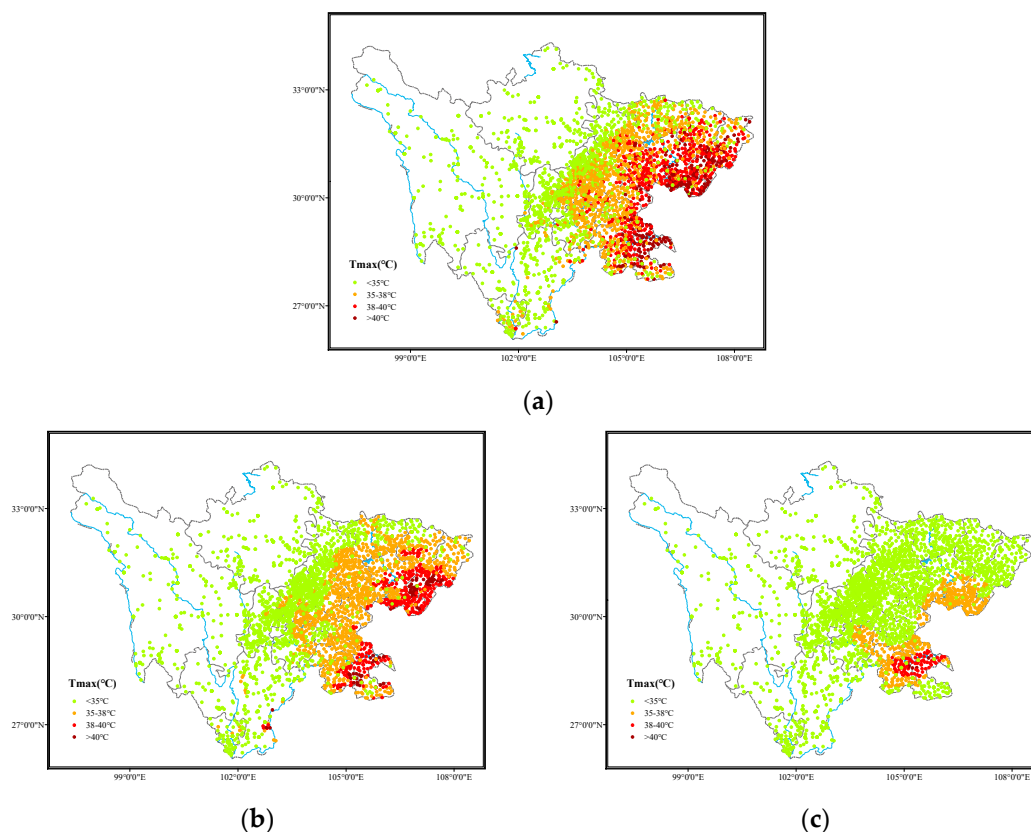


**Figure 15.** Geographic distributions of high temperature stations in Sichuan Province on 20 July in 2018. (a) Observations; (b) CLDAS; (c) GLDAS.

#### 4. Discussion

Near-surface air temperature is an important element in agriculture, ecology, hydrology, environment and other fields. Gridded datasets can make up for the shortage of observations from different sources. It is very necessary to carry out the comprehensive assessment of gridded near-surface air temperature data over major land of China. In this study, the bilinear interpolation method was used to evaluate the performance of CLDAS and GLDAS gridded fusion datasets over major land of China from 2010 to 2015. The COR, bias, MAE, RMSE and TA were calculated as evaluation indices. Spatial and temporal distributions of these evaluation indices were comprehensively analyzed. In addition, the capability of CLDAS and GLDAS to represent high temperature days in July 2018 was also evaluated.

In terms of the spatial variation of near-surface air temperature, both CLDAS and GLDAS were objective and reasonable. However, in southwest China, especially in high altitude areas, CLDAS shows

more detailed local variations, while GLDAS presents more spatially smoothed features. The near-surface air temperature of CLDAS and GLDAS have the same seasonal variation trend. The diurnal variations of both CLDAS and GLDAS was basically consistent with observations. However, CLDAS was generally closer to observations with higher COR, lower RMSE and smaller bias.

The administrative regions in China are divided into four levels: province, city, county and town, among which province was the highest-level administrative division unit. In the context of climate change, the formulation of relevant policies in each province was not the same. Therefore, it was necessary to understand the data quality of CLDAS and GLDAS from the perspective of provinces, so as to help different provinces to select and apply datasets in a targeted way and formulate relevant policies on economic development in the context of climate change. At the same time, the division of provinces in China is based on natural geographical attributes such as mountains and rivers, which are also closely related to climate division. Therefore, it was very necessary to take the province as a unit for datasets assessment, which can not only show more detailed reference basis from the application point of view, but also take into account different types of ecological climate. Evaluation results indicate that the near-surface air temperature of CLDAS was closer to observations than that of GLDAS in all provinces and at all altitudes. On most stations, CLDAS have higher COR, lower RSME and smaller bias than GLDAS. The assessment of near-surface air temperature of other datasets has also been carried out in China [36]. The results show that the near-surface air temperature data quality of European Center for Medium-Range Weather Forecasts (ECMWF) was better than that of Global Forecast System (GFS) and Japan Meteorological Agency (JMA) in general, but from the assessment indicators, the performance of ECMWF, GFS and JMA in China was not as good as that of CLDAS in this study.

The near-surface air temperature of GLDAS was generally reliable over plains of China, but it has large negative bias in complex terrain area and high-elevation area. For both CLDAS and GLADAS, the data quality was better in eastern China than in western China and the accuracy gradually decreases with the increase of altitude. Similar assessment results also appear in high altitude areas of Zhejiang Province [37]. Overall, in high elevation region, complex terrain area and areas with sparse observations, the error was relatively high at certain individual stations. These stations are often located in canyon areas with complex terrain and large elevation variation, which may cause problems in the representativeness of the stations. Therefore, more caution was necessary when using the data in these areas.

Evaluation of daily maximum and minimum temperature indicates that CLDAS was closer to observations than GLDAS in both maximum and minimum temperature. The assessment of GLDAS maximum temperature in the U.S. region shows that GLDAS can reflect the temperature change, but quality of GLDAS in extreme high temperature needs to be further improved [12].

CLDAS was well indicative of high temperature ranging from 35 °C to 38 °C and can well illustrate the high temperature distribution as the areas of high-temperature shown in CLDAS were basically the same as that shown in observations. However, GLDAS cannot realistically represent the high temperature distribution. The areas with extreme high temperature ranging from 38 °C to 40 °C and above 40 °C in both CLDAS and GLDAS were smaller than that in observations. Possible reasons are as follows: First, the attribute and representativeness of data from different sources were different. The value of a grid point in a gridded product was the average value within a certain area (determined by the spatial resolution of the data) around the grid point, while a station observation represents the value at exactly the location of the station. Second, in the comparison of gridded data and in situ observations, the data must be spatially matched (bilinear interpolation was used in this study) and smoothing cannot be avoided during the interpolation. Third, gridded data especially the CLDAS datasets were fused data produced by integrating background data of numerical models and observations. How well the background data of the numerical models can describe extreme high temperature needs further study.

Comparing the evaluation results from different perspectives, it was found that the quality of CLDAS was better than that of GLDAS, which can be attributed to two main reasons. First, a more advanced multi-grid variational analysis method was adopted for data fusion in the production of CLDAS datasets. The background field and the observation field were gradually fused and assimilated from large scale to small scale for the purpose to obtain optimal fusion result. Second, in the development of CLDAS datasets, the high-resolution numerical forecast products from the European Center for Medium Range Weather Forecast were used as the background data, and the data collected at more than 30,000 automatic temperature observation stations deployed by the China Meteorological Administration were used as the observation data. The use of the above two datasets guarantees the quality of the CLDAS temperature product in China. However, this study only evaluates the gridded datasets over a limited period of time, which may not accurately demonstrate the characteristics of evaluation for certain climatic states. Furthermore, the evaluation result was relatively poor for high-elevation stations, and thus, how to correct the results at these stations is an issue that needs further study.

## 5. Conclusions

Although the near-surface air temperature of CLDAS and GLDAS have many common characteristics and can accurately reflect the general features over major land areas of China, important differences were identified in the present study. The spatial details in high mountainous areas were not sufficiently displayed in GLDAS. The near-surface air temperature of CLDAS were more significantly correlated with observations than that of GLDAS and the RMSE and bias were smaller on annual, daily scales and site spatial scale based on the observations. The daily maximum and minimum temperature of CLDAS is closer to observations than that of GLDAS. In particular, the areas of high temperature above 35 °C in CLDAS were basically consistent with the actual situation, implying that CLDAS can better illustrate the high temperature distribution. These differences arise from multiple factors, including different resolutions, different underlying data and different algorithms for combining these data. Comparing the evaluation results from different perspectives, it is found that the quality of CLDAS is better than that of GLDAS over major land of China. However, despite the high quality of CLDAS datasets, the time series of CLDAS datasets is not long enough for climatological analysis. Meanwhile, the CLDAS datasets mainly cover China and its surrounding areas, whereas the GLDAS datasets were long-term global datasets. Therefore, appropriate products should be selected according to different applications.

**Author Contributions:** All authors have read and agree to the published version of the manuscript. Conceptualization, S.H., B.L. and C.S.; methodology, S.H., B.L. and C.S.; software, S.S.; validation, Y.L.; data curation, M.Q.; writing—original draft preparation, S.H.; writing—review and editing, S.H., B.L. and C.S.; visualization, M.Q.; supervision, Y.L.; project administration, B.L. and C.S.; funding acquisition, B.L. and C.S.

**Funding:** This research was funded by the National Key Research and Development Program of China (No. 2017YFC1502804) and the National Key Research and Development Program of China (No. 2018YFC1506601).

**Conflicts of Interest:** The authors declare no conflict of interest.

## References

1. Ko, Y.-T. Modeling an innovative green design method for sustainable products. *Sustainability* **2020**, *12*, 3351. [[CrossRef](#)]
2. Hanberry, B.B. Compounded heat and fire risk for future u.S. Populations. *Sustainability* **2020**, *12*, 3277. [[CrossRef](#)]
3. Popescu, C.R.G. Corporate social responsibility, corporate governance and business performance: Limits and challenges imposed by the implementation of directive 2013/34/eu in romania. *Sustainability* **2019**, *11*, 5146. [[CrossRef](#)]

4. Popescu, C.R.G.; Popescu, G.N. An exploratory study based on a questionnaire concerning green and sustainable finance, corporate social responsibility, and performance: Evidence from the romanian business environment. *J. Risk Financ. Manag.* **2019**, *12*, 162. [[CrossRef](#)]
5. Hu, X.L.; Zhao, Z.L.; Zhang, L.; Liu, Z.; Li, S.M.; Zhang, X.D. A high-temperature risk assessment model for maize based on modis l1st. *Sustainability* **2019**, *11*, 6601. [[CrossRef](#)]
6. Maurer, E.P.; Wood, A.W.; Adam, J.C.; Lettenmaier, D.P.; Nijssen, B. A long-term hydrologically-based data set of land surface fluxes and states for the conterminous united states. *J. Clim.* **2002**, *15*, 3237–3251. [[CrossRef](#)]
7. Yang, F.; Lu, H.; Yang, K.; He, J.; Wang, W.; Wright, J.S.; Li, C.W.; Han, M.L.; Li, Y.S. Evaluation of multiple forcing data sets for precipitation and shortwave radiation over major land areas of china. *Hydrol. Earth Syst. Sci.* **2017**, *21*, 5805–5821. [[CrossRef](#)]
8. Liu, Z. Comparison of versions 6 and 7 3-hourly trmm multi-satellite precipitation analysis (tmpa) research products. *Atmos. Res.* **2015**, *163*, 91–101. [[CrossRef](#)]
9. Han, S.; Shi, C.X.; Xu, B.; Sun, S.; Zhang, T.; Jiang, L.P.; Liang, X. Development and evaluation of hourly and kilometer resolution retrospective and real-time surface meteorological blended forcing dataset (smbfd) in china. *J. Meteorol. Res.* **2019**, *33*, 1168–1181. [[CrossRef](#)]
10. Xie, X.; He, J.H.; Qi, L. A review on applicability evaluation of four reanalysis datasets in china. *J. Meteorol. Environ.* **2011**, *27*, 58–65.
11. Zhao, T.B.; Fu, C.B.; Ke, Z.J.; Guo, W.D. Global atmosphere reanalysis datasets: Current status and recent advances. *Adv. Earth Sci.* **2010**, *25*, 242–254.
12. Ji, L.; Senay, G.B.; Verdin, J.P. Evaluation of the global land data assimilation system (gldas) air temperature data products. *J. Hydrometeorol.* **2015**, *16*, 2463–2480. [[CrossRef](#)]
13. Kanamitsu, M.; Ebisuzaki, W.; Wollen, J.; Yang, S.K.; Hnilo, J.J.; Fiorino, M.G.; Potter, G.L. Ncep-doe amip-ii reanalysis (r-2). *Bull. Am. Meteorol. Soc.* **2002**, *83*, 1631–1643. [[CrossRef](#)]
14. Pan, X.D.; Li, X.; Chao, Z.H. Review of research of forcing data for regional scale hydrological model. *Adv. Earth Sci.* **2010**, *25*, 1314–1324.
15. Wallace, J.M.; Gutzler, D.S. Teleconnections in the geopotential height field during the northern hemisphere winter. *Mon. Weather Rev.* **1981**, *109*, 784–812. [[CrossRef](#)]
16. Thompson, D.W.J.; Wallace, J.M. The arctic oscillation signature in the wintertime geopotential height and temperature fields. *Geophys. Res. Lett.* **1998**, *25*, 1297–1300. [[CrossRef](#)]
17. Kalnay, E.; Kanamitsu, M.; Kistler, R.; Collins, W.G.; Deaven, D.; Gandin, L.S.; Iredell, M. Ncep/ncar 40-year reanalysis project. *Bull. Am. Meteorol. Soc.* **1996**, *77*, 437–472. [[CrossRef](#)]
18. Dee, D.P.; Uppala, S.M.; Simmons, A.J.; Berrisford, P.; Poli, P.; Kobayashi, S.; Andrae, U.; Balmaseda, M. The era-interim reanalysis: Configuration and performance of the data assimilation system. *Q. J. R. Meteorol. Soc.* **2011**, *137*, 553–597. [[CrossRef](#)]
19. Kobayashi, C.; Endo, H.; Ota, Y.; Kobayashi, S.; Onoda, H.; Harada, Y.; Onogi, K.; Kamahori, H. Preliminary results of the jra-55c, an atmospheric reanalysis assimilating conventional observations only. *Sci. Online Lett. Atmos. Sola* **2014**, *10*, 2014–2016. [[CrossRef](#)]
20. Shi, C.X.; Jiang, L.P.; Zhang, T.; Xu, B.; Han, S. Status and plans of cma land data assimilation system (cldas) project. *Egu Gen. Assem. Conf. Abstr.* **2014**, *16*, EGU2014-5671.
21. Xia, Y.L.; Hao, Z.C.; Shi, C.X.; Li, Y.H.; Meng, J.; Xu, T.R.; Wu, X.Y.; Zhang, B.Q. Regional and global land data assimilation systems: Innovations, challenges, and prospects. *J. Meteorol. Res.* **2019**, *33*, 159–189. [[CrossRef](#)]
22. Rodell, M.; Houser, P.R.; Jambor, U.; Gottschalck, J.; Mitchell, K.; Meng, C.J.; Arsenault, K.; Cosgrove, B.; Radakovich, J.; Bosilovich, M. The global land data assimilation system. *Bull. Am. Meteorol. Soc.* **2004**, *85*, 381–394. [[CrossRef](#)]
23. Shi, C.X.; Pan, Y.; Gu, J.X.; Xu, B.; Han, S.; Zhu, Z.; Zhang, L.; Sun, S.; Jiang, Z.W. A review of multi-source meteorological data fusion products. *Acta Meteorol. Sin.* **2019**, *77*, 774–783.
24. Shi, C.X.; Xie, Z.H.; Qian, H.; Liang, M.L.; Yang, X.C. China land soil moisture enkf data assimilation based on satellite remote sensing data. *Sci. China Earth Sci.* **2011**, *54*, 1430–1440. [[CrossRef](#)]
25. Wang, H.; Huang, J.J.; Zhou, H.; Zhao, L.X.; Yuan, Y.B. An integrated variational mode decomposition and arima model to forecast air temperature. *Sustainability* **2019**, *11*, 4018. [[CrossRef](#)]

26. Kumar, S.V.; Peters-Lidard, C.D.; Tian, Y.; Houser, P.R.; Geiger, J.; Olden, S.; Lighty, L.; Eastman, J.L.; Doty, B.; Dirmeyer, P. Land information system: An interoperable framework for high resolution land surface modeling. *Environ. Model. Softw.* **2006**, *21*, 1402–1415. [[CrossRef](#)]
27. Rui, H.L.; Beaudoin, H. README Document for GLDAS Version 1 Data Products. Available online: [https://hydro1.gesdisc.eosdis.nasa.gov/data/GLDAS\\_V1/README.GLDAS.pdf](https://hydro1.gesdisc.eosdis.nasa.gov/data/GLDAS_V1/README.GLDAS.pdf) (accessed on 24 May 2020).
28. Rui, H.L.; Beaudoin, H. README Document for NASA GLDAS Version 2 Data Products. Available online: [https://hydro1.gesdisc.eosdis.nasa.gov/data/GLDAS/README\\_GLDAS2.pdf](https://hydro1.gesdisc.eosdis.nasa.gov/data/GLDAS/README_GLDAS2.pdf) (accessed on 24 May 2020).
29. Stamnes, K.; Tsay, S.C.; Wiscombe, W.; Jayaweera, K. Numerically stable algorithm for discrete-ordinate-method radiative transfer in multiple scattering and emitting layered media. *Appl. Opt.* **1988**, *27*, 2502–2509. [[CrossRef](#)]
30. Oleson, K.W.; Niu, G.Y.; Yang, Z.L.; Lawrence, D.M.; Thornton, P.E.; Lawrence, P.J.; Stokli, R.; Dickinson, R.E.; Bonan, G.B.; Levis, S. Improvements to the community land model and their impact on the hydrological cycle. *J. Geophys. Res. Biogeosci.* **2008**, *113*, G01021. [[CrossRef](#)]
31. Dai, Y.J.; Zeng, X.B.; Dickinson, R.E.; Baker, I.; Bonan, G.B.; Bosilovich, M.G.; Denning, S.; Dirmeyer, P. The common land model. *Bull. Am. Meteorol. Soc.* **2001**, *84*, 1013–1023. [[CrossRef](#)]
32. Niu, G.Y.; Yang, Z.L. An observation-based formulation of snow cover fraction and its evaluation over large north american river basins. *J. Geophys. Res.* **2007**, *112*, D21101. [[CrossRef](#)]
33. Han, S. *The Simulation and Evaluation Using ckm3.5 and ssib2 Land Surface Model Based Cldas Forcing data with Drought Monitoring*; Nanjing University of Information Science and Technology: Nanjing, China, 2015.
34. Han, S.; Shi, C.X.; Jiang, L.P.; Zhang, T.; Liang, X.; Jiang, Z.W.; Xu, B.; Li, X.F.; Zhi, Z.; Lin, H.J. The simulation and evaluation of soil moisture based on cldas. *J. Appl. Meteorol. Sci.* **2017**, *28*, 369–378.
35. Ren, Z.H.; Zhang, Z.F.; Sun, C.; Liu, Y.M.; Li, J.; Ju, X.H.; Zhao, Y.F.; Li, Z.P.; Zhang, W.; Li, H.K.; et al. Development of three-step quality control system of real-time observation data from aws in china. *Meteorol. Mon.* **2015**, *41*, 1268–1277.
36. Gong, W.W.; Shi, C.X.; Zhang, T.; Jiang, L.P.; Zhuang, Y.; Meng, X.Y. Evaluation of surface meteorological elements from several numerical models in china. *Clim. Environ. Res.* **2015**, *20*, 53–62.
37. Chen, F.; Yang, X.C.; Ji, C.X.; Li, Y.J.; Deng, F.P.; Dong, M.Y. Establishment and assessment of hourly high-resolution gridded air temperature data sets in zhejiang, china. *Meteorol. Appl.* **2019**, *26*, 396–408. [[CrossRef](#)]

